

---

## V.E.4 Performance and Durability of Advanced Automotive Fuel Cell Stacks and Systems with Dispersed Alloy Cathode Catalyst in Membrane Electrode Assemblies

Rajesh K. Ahluwalia (Primary Contact),  
Xiaohua Wang, and J-K Peng

Argonne National Laboratory  
9700 South Cass Avenue  
Argonne, IL 60439  
Phone: (630) 252-5979  
Email: walia@anl.gov

DOE Manager: Nancy L. Garland  
Phone: (202) 586-5673  
Email: Nancy.Garland@ee.doe.gov

Project Start Date: October 1, 2003  
Project End Date: Project continuation and direction  
determined annually by DOE

### Overall Objectives

- Develop a validated model for automotive fuel cell systems, and use it to assess the status of the technology.
- Conduct studies to improve performance and packaging, to reduce cost, and to identify key research and development issues.
- Compare and assess alternative configurations and systems for transportation and stationary applications.
- Support DOE/U.S. DRIVE automotive fuel cell development efforts.

### Fiscal Year (FY) 2017 Objectives

- Quantify the impact of low-platinum group metal (PGM) alloy catalysts and alternate catalyst supports on the performance of automotive stacks and fuel cell systems.
- Understand the durability of low-PGM alloy catalysts under cyclic potentials.
- Extend system analysis to non-nanostructured thin film (NSTF) membrane electrode assemblies (MEAs) with conventional Pt/C and advanced Pt alloy/C cathode catalysts.
- Incorporate durability considerations in system analysis.

- Provide modeling support to Strategic Analysis, Inc., in annual update of progress in meeting technical targets including fuel cell system (FCS) cost.

### Technical Barriers

This project addresses the following technical barriers from the Fuel Cells section of the Fuel Cell Technologies Office Multi-Year Research, Development, and Demonstration Plan.

- (A) Durability
- (B) Cost
- (C) Performance

### Technical Targets

This project is conducting system level analyses to address the following DOE 2020 technical targets for automotive fuel cell power systems operating on direct hydrogen.

- Energy efficiency: 60% at 25% of rated power
- $Q/\Delta T$ : 1.45 kW/°C
- Power density: 850 W/L for system, 2,500 W/L for stack
- Specific power: 850 W/kg for system, 2,000 W/kg for stack
- Transient response: 1 s from 10% to 90% of maximum flow
- Start-up time: 30 s from -20°C and 5 s from +20°C ambient temperature
- Precious metal content: 0.125 g/kW<sub>e</sub> rated gross power

### Accomplishments

- Projected \$44.9/kW<sub>e</sub> FCS cost at high volume manufacturing and 0.126 g/kW<sub>e</sub> Pt content with high performance d-PtNi/C cathode catalyst, reinforced 14- $\mu$ m 850 equivalent weight (EW) membrane, and  $Q/\Delta T = 1.45$  kW/°C constraint.
- Estimated 10% degradation in net FCS power with 40% decrease in d-PtNi/C cathode catalyst electrochemical surface area (ECSA) (0.05–0.15 mg/cm<sup>2</sup> Pt loading) due to cyclic potentials.

- Showed the possibility of removing cathode humidifier if MEA membrane is <14- $\mu\text{m}$  thick, and stack inlet pressure is 2.5 atm or higher.
- Demonstrated through a computational fluid dynamic model that  $\text{H}_2$  recirculation blower can be eliminated by using a pulse ejector and maintaining <20%  $\text{N}_2$  mole fraction to avoid fuel starvation.
- Evaluated extreme conditions (cell voltage, manufacturing volume,  $Q/\Delta T$  constraint) where high stack inlet pressures (4 atm) may offer advantages.



## INTRODUCTION

While different developers are addressing improvements in individual components and subsystems in automotive fuel cell propulsion systems (i.e., cells, stacks, balance-of-plant components), we are using modeling and analysis to address issues of thermal and water management, design-point and part-load operation, and component-, system-, and vehicle-level efficiencies and fuel economies. Such analyses are essential for effective system integration.

## APPROACH

Two sets of models are being developed. The GCtool software is a stand-alone code with capabilities for design, off-design, steady state, transient, and constrained optimization analyses of FCS. A companion code, GCtool-ENG, has an alternative set of models with a built-in procedure for translation to the MATLAB/SIMULINK platform commonly used in vehicle simulation codes, such as Autonomie.

## RESULTS

We implemented a formal methodology for developing an integral cell model using differential cell data [1]. As outlined in Figure 1a, it consists of taking polarization data at different operating conditions, and determining the cathode catalyst layer (CCL) ionic conductivity ( $\sigma_c$ ) and high-frequency resistance ( $R_Q^m$ ) from the impedance (EIS) data in  $\text{H}_2/\text{N}_2$  and Pt oxide formation ( $\theta$ ) and kinetics from the cyclic voltammetry data. Knowing  $\sigma_c$  and  $\theta$ , a model for distributed oxygen reduction reaction (ORR) kinetic ( $\eta_c^f$ ) and ionic overpotentials ( $iR_Q^c$ ) is constructed using the low current density ( $i$ ) polarization data at different pressures (P), temperatures (T),  $\text{O}_2$  mole fraction ( $X_{\text{O}_2}$ ) and relative humidity (RH). Next, the complete set of polarizations is analyzed to determine the mass transfer overpotentials ( $\eta_m$ ) at high current densities and to correlate  $\eta_m$  in terms of limiting current density ( $i_l$ ). Together with ORR kinetic model,  $\eta_m$  correlation can be used in a finite difference model

to predict the performance of large integral cells operating non-isothermally at finite stoichiometry with co- or counter-current anode, cathode and coolant flows. Alternatively,  $\eta_m$  correlation can be used to distinguish the individual contributions of gas channel ( $R_g$ ), gas diffusion layer ( $R_d$ ), and CCL ( $R_c$ ) to the overall  $\text{O}_2$  mass transport resistance ( $R_m$ ).

We used the above methodology to determine the mass activity and kinetics of different Pt and Pt alloy catalyst systems for ORR. All the dispersed catalysts in this study used the same high surface-area carbon support, i.e., Ketjen black. Table 1 summarizes the measured mass activities for ORR in  $\text{H}_2/\text{O}_2$  at 0.9 V (internal resistance [IR]-free), 1-atm  $\text{O}_2$  partial pressure, 80°C and 100% RH. It also includes the modeled activities derived from the polarization data at low current densities in  $\text{H}_2/\text{air}$  and  $\text{H}_2/\text{O}_2$ . The important results from this study are briefly discussed below.

- Annealing (a) highly dispersed Pt/C catalyst grows the median size of the nanoparticles from 2–3 nm to 4–5 nm, and reduces ECSA by ~47% [2]. The resulting ~28% decrease in mass activity is less than the reduction in ECSA because the specific activity is higher for larger nanoparticles.
- De-alloyed (d)  $\text{PtNi}_3/\text{C}$  catalyst has undergone the same thermal treatment as a-Pt/C catalyst, has nearly the same particle size, but has 40–100% higher mass activity [2]. The wide disparity in mass activity data is due to variability in samples with different ionomer EW and I/C ratio.
- PtCo/C alloy catalysts have mass activities comparable to d-PtNi/C. The three PtCo/C catalyst systems listed in Table 1 had similar mass activities even though they had different electrode microstructures and the Co contents varied over a wide range [3]. Transmission electron microscopy analysis of the high-Co content (H) catalyst electrode, 0.2  $\text{mg}/\text{cm}^2$  Pt loading, showed a “spongy” porous (hollow) catalyst nanoparticle morphology with ~6.7 nm median Pt-Co particle size after conditioning. The medium-Co content (M) catalyst electrode, 0.1  $\text{mg}/\text{cm}^2$  Pt loading, showed a crystalline fully alloyed catalyst nanoparticle morphology with ~4.4 nm particle size after conditioning. The low-Co content (L) catalyst electrode, 0.1  $\text{mg}/\text{cm}^2$  Pt loading, also showed catalysts with a fully alloyed crystalline morphology with ~4.5 nm median particle size.
- Binary d- $\text{Pt}_3\text{Ni}_7/\text{NSTF}$  catalyst has 80–100% higher mass activity than the baseline  $\text{Pt}_{68}(\text{CoMn})_{32}/\text{NSTF}$  catalyst [4,5]. Higher ECSA and improved specific activity contribute almost equally to the increase in mass activity of the binary NSTF catalyst over the baseline ternary catalyst. Addition of the dispersed Pt/C cathode interlayer increases ECSA but does not improve the mass activity.

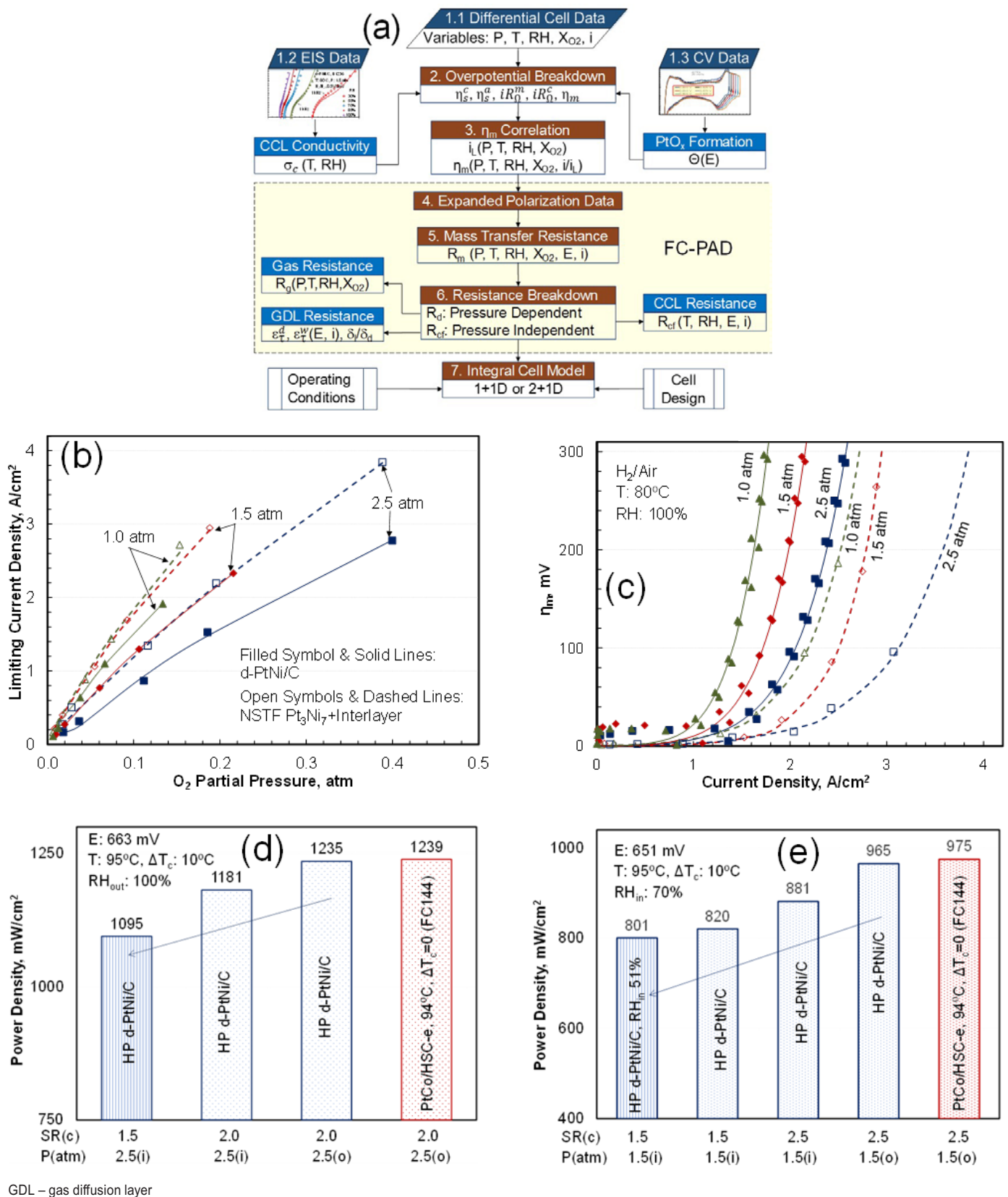


**FIGURE 1.** Stack model development methodology and calibration: (a) methodology for development of integral cell model using differential cell data; (b) dispersed and NSTF electrodes:  $i_l$ ; (c) dispersed and NSTF electrodes:  $\eta_m$ ; (d) calibration of d-PtNi/C cathode model at 2.5 atm; (e) calibration of d-PtNi/C cathode model at 1.5 atm

**TABLE 1.** Mass Activities of Pt and Pt Alloy Catalyst Systems [2–5]

Cathode Catalyst	Ionomer		Cathode		Mass Activity	
	EW (l/c)	$L_{Pt}(c)$ mg/cm <sup>2</sup>	ECSA m <sup>2</sup> /g	Data A/g <sub>Rt</sub>	Model A/g <sub>Rt</sub>	
<b>Dispersed De-alloyed Catalyst (FC106, 12.25-cm<sup>2</sup> cell)</b>						
d-PtNi <sub>3</sub> /C	850 (1.0)	0.1	64±11	500±100	650±120	
<b>Baseline Annealed Pt Catalysts (FC106, 12.25-cm<sup>2</sup> cell)</b>						
a-Pt/C	1100 (0.8, 1.2)	0.104	48±4	312±24	319±30	
<b>Baseline Dispersed Pt Catalysts (FC106, 12.25-cm<sup>2</sup> cell)</b>						
Pt/C	1100 (0.8)	0.092	90±8	432±22	456	
<b>Dispersed PtCo Catalysts (FC-PAD, 50-cm<sup>2</sup> cell)</b>						
Pt <sub>60</sub> Co <sub>40</sub> /C	(0.34)	0.21	42.4	745	763	
Pt <sub>70</sub> Co <sub>30</sub> /C	(0.9)	0.1	42.4±0.7	659	623	
Pt <sub>85</sub> Co <sub>15</sub> /C	(0.9)	0.1	42.4	760	661	
<b>NSTF Catalysts (FC104, 50-cm<sup>2</sup> cells, 5-cm<sup>2</sup> for binary catalyst with CI)</b>						
Pt <sub>68</sub> (CoMn) <sub>32</sub> /NSTF	None	0.1	9.8	180	190	
d-Pt <sub>3</sub> Ni <sub>7</sub> /NSTF	None	0.125	14.5±0.7	330±30	392	
d-Pt <sub>3</sub> Ni <sub>7</sub> /NSTF + Cathode Interlayer (CI)	None	0.096 + 0.016 (CI)	22±3	380±60	334	

- The modeled mass activity can be different than the measured values, up to 50% for d-PtNi<sub>3</sub>/C. However, the calculated polarization curves for H<sub>2</sub>/air in the kinetic region using the modeled mass activity and other kinetic constants are in good agreement with the experimental data.

We also used the above methodology to determine the limiting current densities ( $i_L$ ) and mass transfer overpotentials ( $\eta_m$ ) for the alloy catalyst systems listed in Table 1. Figures 1b and 1c compare  $i_L$  and  $\eta_m$  for the dispersed d-PtNi<sub>3</sub>/C and binary d-Pt<sub>3</sub>Ni<sub>7</sub>/NSTF electrodes in differentials cells. At 80°C,  $i_L$  are considerably higher and  $\eta_m$  are significantly lower in the thin NSTF electrode (<1 μm thick) than the thick dispersed catalyst electrode (~7–10 μm thick).

We calibrated the performance model for d-PtNi/C cathode catalyst with 50-cm<sup>2</sup> cell data for d-PtCo/C catalyst, finite cathode/anode stoichiometry and operating temperature needed to satisfy the Q/ΔT constraint [6]. Figure 1c shows the measured power densities for PtCo/C alloy catalysts at 95°C and 100% outlet RH for two combinations of outlet pressures and cathode stoichiometry (SR), 1239 mW/cm<sup>2</sup> at 663 mV, 2.5 atm and SR(c) = 2.0, and 975 mW/cm<sup>2</sup> at 652 mV, 1.5 atm and SR(c) = 2.5. Also shown are modeled results for PtNi/C alloy catalyst that has similar ECSA, mass activity and Pt loadings, 0.025/0.1 mg/cm<sup>2</sup> on anode/cathode, and 10°C rise in coolant temperature (ΔT<sub>c</sub>). The chemically-stabilized reinforced membrane (14-μm dry thickness, 850 EW) was chosen to have similar high frequency resistance, ~42 mΩ.cm<sup>2</sup>. The model was aligned with the experimental data by increasing the limiting current density by 20% to reflect more accessible pores in the high surface-area carbon support for the PtCo/C alloy catalyst. The modeled electrode sheet resistance compares well with the measured value, 47 mΩ.cm<sup>2</sup> at 100% RH. System analysis results are generally quoted at specified stack inlet rather than outlet pressures in which case the model indicates 4.4% decrease in power density at 2.5 atm and 8.7% decrease at 1.5 atm. System analysis shows lower FCS cost at SR(c) = 1.5 for which SR(c) the modeled power density further decreases by 7.3% to 1,095 mW/cm<sup>2</sup> at 2.5 atm and by 6.9% to 820 mW/cm<sup>2</sup> at 1.5 atm. System analysis also shows lower FCS cost under drier conditions (70% outlet RH) for 1.5 atm stack inlet pressure in which case the power density further decreases by 2.3% to 801 mW/cm<sup>2</sup>.

Figure 2 summarizes the projected cost (\$/kW<sub>e</sub>) and performance (g<sub>Pt</sub>/kW<sub>e</sub>) of 80-kW<sub>e</sub> FCS with d-PtNi alloy catalyst supported on high surface area carbon with accessible pores as in Figure 1c. At 2.5 atm stack inlet

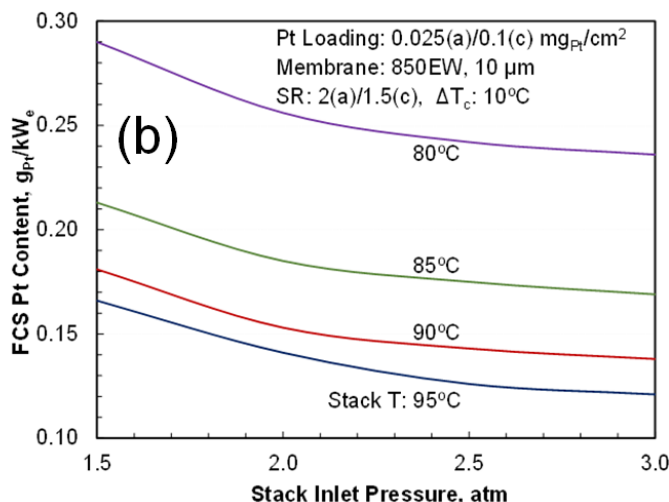
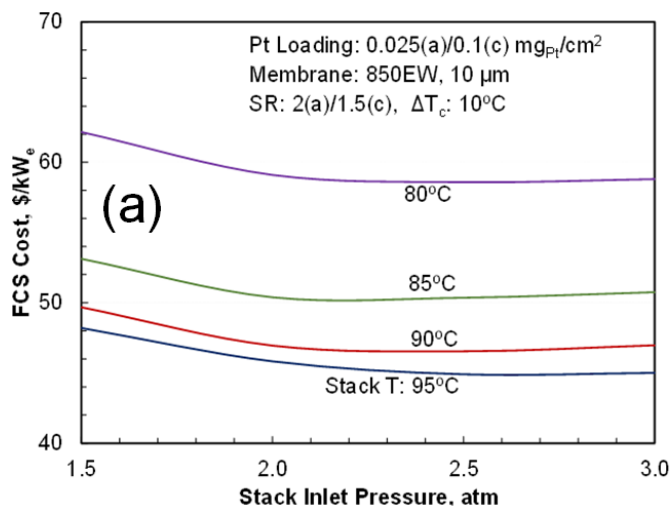


**FIGURE 2.** Projected cost and performance of automotive fuel cell systems with de-alloyed cathode catalyst: (a) projected cost of FCS with d-PtNi/C cathode; (b) projected Pt content with d-PtNi/C cathode

pressure, the projected cost at high volume manufacturing (500,000 units/yr) is less than \$45/kW<sub>e</sub> [7] and the stack Pt content exceeds the 2020 target of 0.125 g<sub>Pt</sub>/kW<sub>e</sub> (see Table 2). Pending demonstration in full-size stacks, these results are considered landmark accomplishments for automotive fuel cell systems.

**TABLE 2.** Projected Performance of Air Management Subsystem, Stack, and FCS

T: 95°C		Stack Gross				FCS Net	
P	CEM Power	Current Density	Cell Voltage	Power Density	Stack Pt Content	Pt Cost	Stack Cost
atm	kW <sub>e</sub>	A/cm <sup>2</sup>	mV	mW/cm <sup>2</sup>	g <sub>Pt</sub> /kW <sub>e</sub>	\$/kW <sub>e</sub>	\$/kW <sub>e</sub>
3.0	8.8	1.735	670	1162	0.108	5.8	18.6
2.5	7.0	1.651	663	1095	0.114	6.1	19.2
2.0	5.5	1.457	657	956	0.131	6.8	21.1
1.5	4.1	1.231	651	801	0.156	8.0	24.2

CEM – compressor-expander-motor

Figure 3 summarizes results of a study to determine the optimum Pt loading in d-PtNi/C cathode. With Q/ΔT= 1.45 kW/°C constraint and bipolar plate temperature restricted to 95°C, the cell voltage is mainly a function of the operating pressure, 663 mV at 2.5 atm and 651 mV at 1.5 atm, and the total overpotential is nearly independent of Pt loading. Figures 3a and 3b show that the current density adjusts such that the mass transfer overpotentials ( $\eta_m$ ) are similar, but the higher cathode overpotentials ( $\eta_c = \eta_c^c + iR_O^c$ ) at lower Pt loadings are compensated by the corresponding lower Ohmic overpotentials ( $iR_O^m$ ). Figures 3c and 3d show that the resulting power density is about 33% lower at 0.05 mg/cm<sup>2</sup> than at 0.15 mg/cm<sup>2</sup> Pt loading but the overall cost differences are small. Thus, even though the overall FCS cost is smallest for 0.10 mg/cm<sup>2</sup> Pt loading in cathode, other factors such as packaging and durability may favor higher Pt loadings.

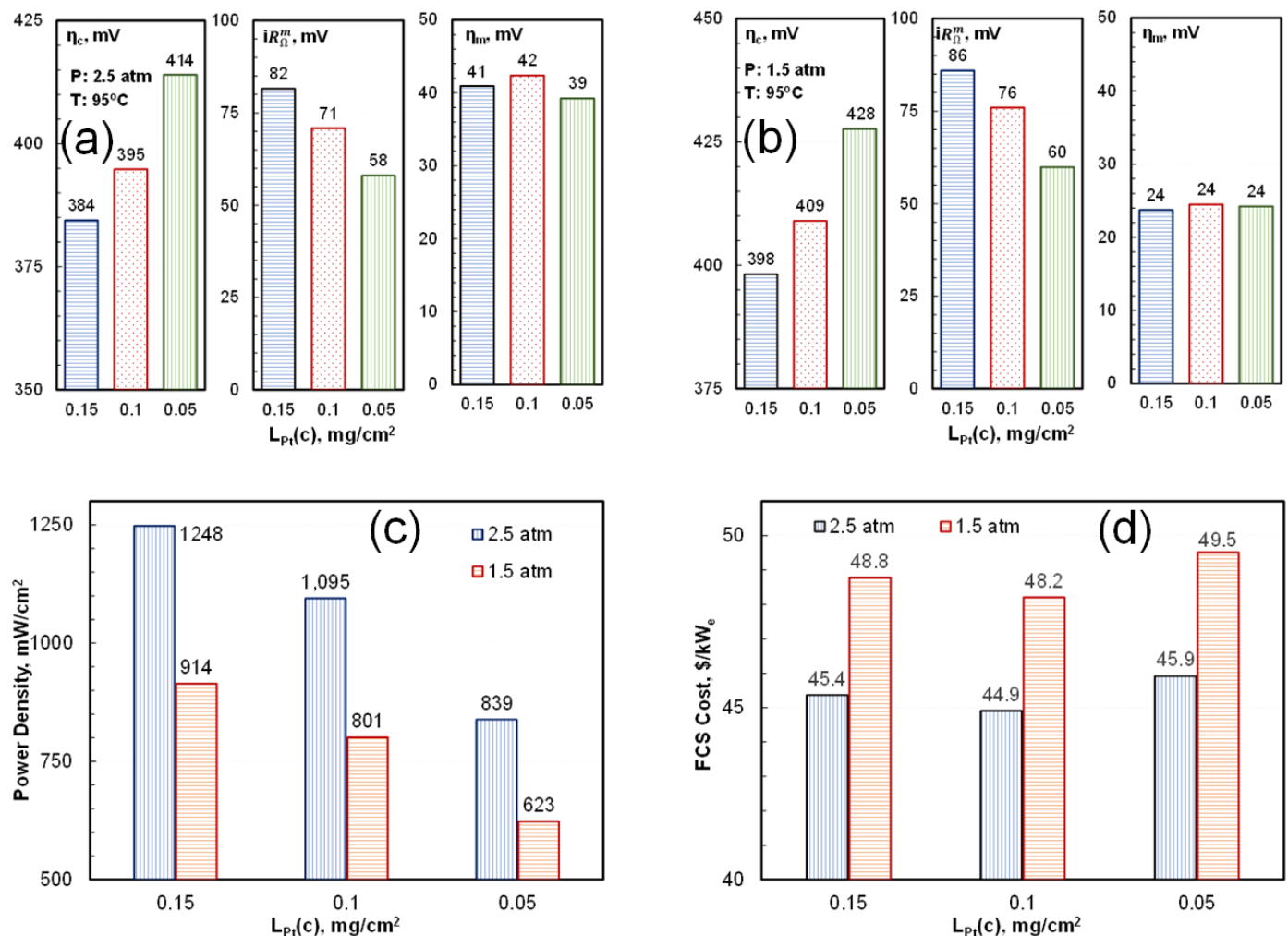


**FIGURE 3.** Optimum Pt loading ( $L_{Pt}$ ) in d-PtNi/C cathode electrode: (a) cell overpotentials, 2.5 atm inlet pressure; (b) cell overpotentials, 1.5 atm inlet pressure; (c) stack power density; (d) projected FCS cost

## Durability of MEAs with d-PtNi/C Catalysts

We investigated the durability of d-PtNi/C electrodes by analyzing the data acquired in FC-106 project [2] using differential cells subjected to 30,000 trapezoid (0.6–0.95 V, 700 mV/s) and triangle (0.6–0.925 V, 50 mV/s) cycles in  $H_2/N_2$ . The trapezoid cycle mimics the new catalyst durability protocol: 0.6 V lower potential limit, 0.95 V upper potential limit, and 700 mV/s scan rate. The triangle cycle shares many features of the old catalyst durability protocol: 0.6 V lower potential limit, 0.925 V upper potential limit, and 50 mV/s scan rate. Figure 4a shows that catalyst durability, as characterized by transition metal and ECSA retention, is worse under the trapezoid cycle that has higher upper potential limit and scan rate than the triangle cycle. Extensive intra-cycle diagnostics also has adverse impact on catalyst durability.

Wide angle X-ray scattering measurements indicate extensive leaching of the transition metal (Ni) that depends on the duty cycle in much the same way as ECSA loss, although the mechanisms are entirely different. Even with >90% Ni loss from the alloy catalyst, Figure 4b indicates <10% degradation in catalyst specific activity (SA), suggesting that only a small amount of Ni may be needed in alloy to enhance the ORR activity of Pt catalysts. Besides Ni loss, degradation in SA should also depend on growth of catalyst particle size with cycling. Lacking sufficient data and recognizing that ECSA loss ( $\Delta A_{Pt}$ ) is related to Ni loss and particle size growth, we find it convenient to correlate the degradation in SA with  $\Delta A_{Pt}$ .

Figure 4c shows the correlation in mass activity degradation with ECSA loss. The degradation in mass activity (product of SA and  $A_{Pt}$ ) is more than linear with  $\Delta A_{Pt}$  because, as noted above, SA also decreases with ECSA loss.

Employing procedures developed earlier, we determined the limiting current densities ( $i_l$ ) and mass transfer overpotentials ( $\eta_m$ ) for d-PtNi/C electrodes using the polarization curves obtained at beginning of test and after 30,000 potential cycles. Figure 4d shows that the effect of potential cycling on limiting current density can be captured by correlating with catalyst roughness ( $S_{Pt}$ ) which is the product of ECSA and Pt loading.

Using the data in Figures 4b–4d, we conducted system analysis to determine the acceptable loss in ECSA to satisfy the target of limiting net FCS power loss to less than 10% after 5,000 h. Figure 4e presents FCS net power, 80 kW<sub>e</sub> at beginning of life, as a function of  $\Delta A_{Pt}$  for three Pt loadings in d-PtNi/C cathodes. We conclude that the target of 10% derating in net FCS power over lifetime can be met by limiting ECSA loss to <40% for 0.1 mg/cm<sup>2</sup> Pt loading in cathode. There is only a small dependence of acceptable ECSA loss on Pt loading although Pt loading may affect ECSA loss over cyclic potentials and during

startup/shutdown. Regardless of Pt loading, Figure 4f shows that increase in kinetic and mass transfer overpotentials contribute equally to voltage loss. Future work will consider additional degradation mechanisms involving other components (membrane, catalyst support) and fuel/air impurities.

## CONCLUSIONS AND UPCOMING ACTIVITIES

- We have formalized a methodology for developing an integral cell model using differential cell data. It provides a consistent basis for determining ORR kinetic parameters, mass transfer overpotentials, and distinguishing  $O_2$  mass transfer resistances in the gas channel, diffusion medium and cathode catalyst layer.
- We demonstrated that a low-PGM alloy catalyst (0.125 mg/cm<sup>2</sup> total Pt loading in anode and cathode) supported on an advanced high surface area carbon support with tailored pore size distribution can achieve power densities exceeding the 2020 target of 1,000 mW/cm<sup>2</sup> at lower than 0.125 g/kW<sub>e</sub> PGM content under operating conditions (95°C, <100% outlet RH, SR(c) = 1.5, 2.5 atm stack inlet pressure) required to meet the heat rejection constraint ( $Q/\Delta T$ : 1.45 kW/°C).
- Analysis of the complete fuel cell system with the above alloy catalyst and carbon support and passive anode gas recirculation leads us to project \$45/kW<sub>e</sub> FCS cost at high volume manufacturing. Pending demonstration in full-size stacks, these results are considered landmark accomplishments for automotive fuel cell systems.
- We developed a model for alloy catalyst durability under cyclic potentials and used it to determine the acceptable loss in ECSA to satisfy the target of limiting net FCS power loss to less than 10% after 5,000 h. We concluded that the target of 10% derating in net FCS power over lifetime can be met by limiting ECSA loss to <40% for 0.1 mg/cm<sup>2</sup> Pt loading in cathode. There is only a small dependence of acceptable ECSA loss on Pt loading although Pt loading may affect ECSA loss over cyclic potentials and during startup/shutdown.
- Our future work will focus on verifying the above conclusions by obtaining differential cell data with d-PtCo/C catalyst supported on surface area carbon with tailored pore size distribution. We will also analyze the durability of this catalyst system under cyclic potentials.

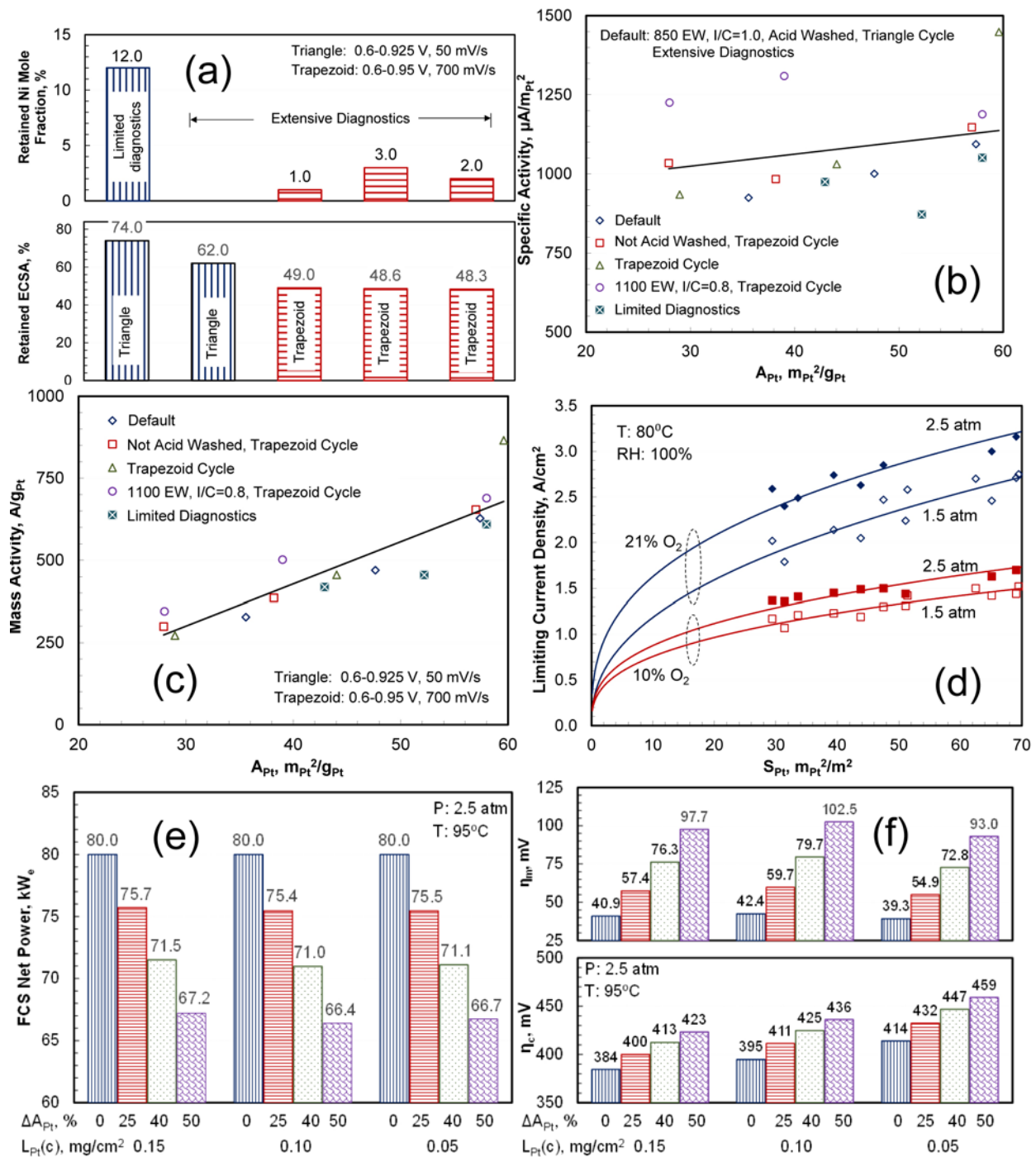


**FIGURE 4.** Stability of alloy catalysts and projected FCS performance degradation: (a) retention of transition metal and ECSA under cyclic potentials; (b) specific activity degradation; (c) mass activity degradation; (d) limiting current density degradation; (e) performance degradation; (f) increase of overpotentials with aging

## FY 2017 PUBLICATIONS/PRESENTATIONS

1. R.K. Ahluwalia, X. Wang, and A.J. Steinbach, “Performance of Advanced Automotive Fuel Cell Systems with Heat Rejection Constraint,” *Journal of Power Sources*, Vol. 309, pp. 178–191, 2016.

2. R.K. Ahluwalia, J.-K. Peng, X. Wang, D.A. Cullen, and A.J. Steinbach, “Long-Term Stability of Nanostructured Thin Film Electrodes at Operating Potentials,” *Journal of the Electrochemical Society*, Vol. 164(4), pp. F306–F320, 2017.

3. F.C. Cetinbas, R.K. Ahluwalia, N. Kariuki, et al., “Hybrid Approach Combining Multiple Characterization Techniques and

Simulations for Microstructural Analysis of Proton Exchange Membrane Fuel Cell Electrodes,” *Journal of Power Sources*, Vol. 344, pp. 62–73, 2017.

4. R.K. Ahluwalia, X. Wang, J-K Peng, and C.F. Cetinbas, “Fuel Cells Systems Analysis,” U.S. DRIVE Fuel Cell Tech Team Meeting, Southfield, MI, May 18, 2016.
5. C.F. Cetinbas, R.K. Ahluwalia, N. Kariuki, D.J. Myers, V.J. De Andrade, “Hybrid Approach for PEM Fuel Cell Electrode Microstructural Analysis,” ElectroCat Workshop, Argonne National Laboratory, Argonne, IL, July 26, 2016.
6. D. Myers, N. Kariuki, R. Ahluwalia, X. Wang, C.F. Cetinbas, and J.-K. Peng, “Performance and Stability of MEA for PEMFC with Pt Alloy Cathode Catalyst,” IEA Annex 34 Meeting, Beijing, China, November 9, 2016.
7. R.K. Ahluwalia, V. Weissbecker, C. Wang, S. Hirano, H. Bramfeldt, and H. Ljungcrantz, “Bipolar Plates for Automotive Fuel Cells: Annex 34 Summary Report,” IEA Annex 34 Meeting, Beijing, China, November 9, 2016.
8. R.K. Ahluwalia and N.L. Garland, “Reports from the Annexes: Annex 34,” IEA AFC ExCo 53rd Meeting, Beijing, China, November 10–11, 2016.
9. R.K. Ahluwalia, D.D. Papadias, X. Wang, R. Borup, R. Mukundan, M. Brady, J. Thompson, H. Wang, and J. Turner, “Modeling Performance and Stability of Bipolar Plates for Automotive Fuel Cells,” DOE 2017 Bipolar Plates Workshop, Southfield, MI, February 14, 2017.
10. R. Borup, R. Mukundan, T. Rockward, M. Brady, J. Thompson, D.D. Papadias, R.K. Ahluwalia, H. Wang, and J. Turner, “Metal Bipolar Plate Testing,” DOE 2017 Bipolar Plates Workshop, Southfield, MI, February 14, 2017.
11. R.K. Ahluwalia, “IEA Advanced Fuel Cells Annex 34: Fuel Cells for Transportation,” Beijing, China, November 9, 2016.

## REFERENCES

1. R.K. Ahluwalia, X. Wang, and A.J. Steinbach, “Performance of Advanced Automotive Fuel Cell Systems with Heat Rejection Constraint,” *J. Power Sources* 309 (2016) 178–191.
2. D.J. Myers, N. Kariuki, R.K. Ahluwalia, X. Wang, C.F. Cetinbas, and J-K Peng, “Rationally Designed Catalyst Layers for PEMFC Performance Optimization,” DOE Hydrogen and Fuel Cells Program, FY 2016 Annual Progress Report, DOE/Go-102017-4891, V.D.3, 1–5.
3. S.S. Kocha, J. Christ, et al., “FC-PAD: Electrode Layer Integration,” DOE Hydrogen and Fuel Cells Program, FY 2016 Annual Progress Report DOE/Go-102017-4891, V.D.1, 1–6.
4. A.J. Steinbach, A. Hester, et al., “High Performance, Durable, Low Cost Membrane Electrode Assemblies for Transportation Applications,” DOE Hydrogen and Fuel Cells Program, FY 2016 Annual Progress Report, DOE/Go-102017-4891, V.B.3, 1–6.
5. R.K. Ahluwalia, X. Wang, and J-K Peng, “Performance and Durability of Advanced Automotive Fuel Cell Stacks and Systems with Nanostructured Thin Film Catalyst Based Membrane Electrode Assemblies,” DOE Hydrogen and Fuel Cells Program, FY 2016 Annual Progress Report, DOE/Go-102017-4891, V.F.5, 1–8.
6. A. Kongkanand, “Highly Accessible Catalysts for Durable High-Power Performance,” DOE Hydrogen and Fuel Cells Program, 2017 Annual Merit Review and Evaluation Meeting, FC144, Washington, DC, June 5–9, (2017).
7. B.D. James, J.M. Huya-Kouadio, C. Houchins, and D.A. DeSantis, “Fuel Cell Vehicle and Bus Cost Analysis,” DOE Hydrogen and Fuel Cells Program, FY 2016 Annual Progress Report, DOE/Go-102017-4891, V.F.6, 1–5.